
Figures and figure supplements

Structure of *Dunaliella* photosystem II reveals conformational flexibility of stacked and unstacked supercomplexes

Ido Caspy et al.

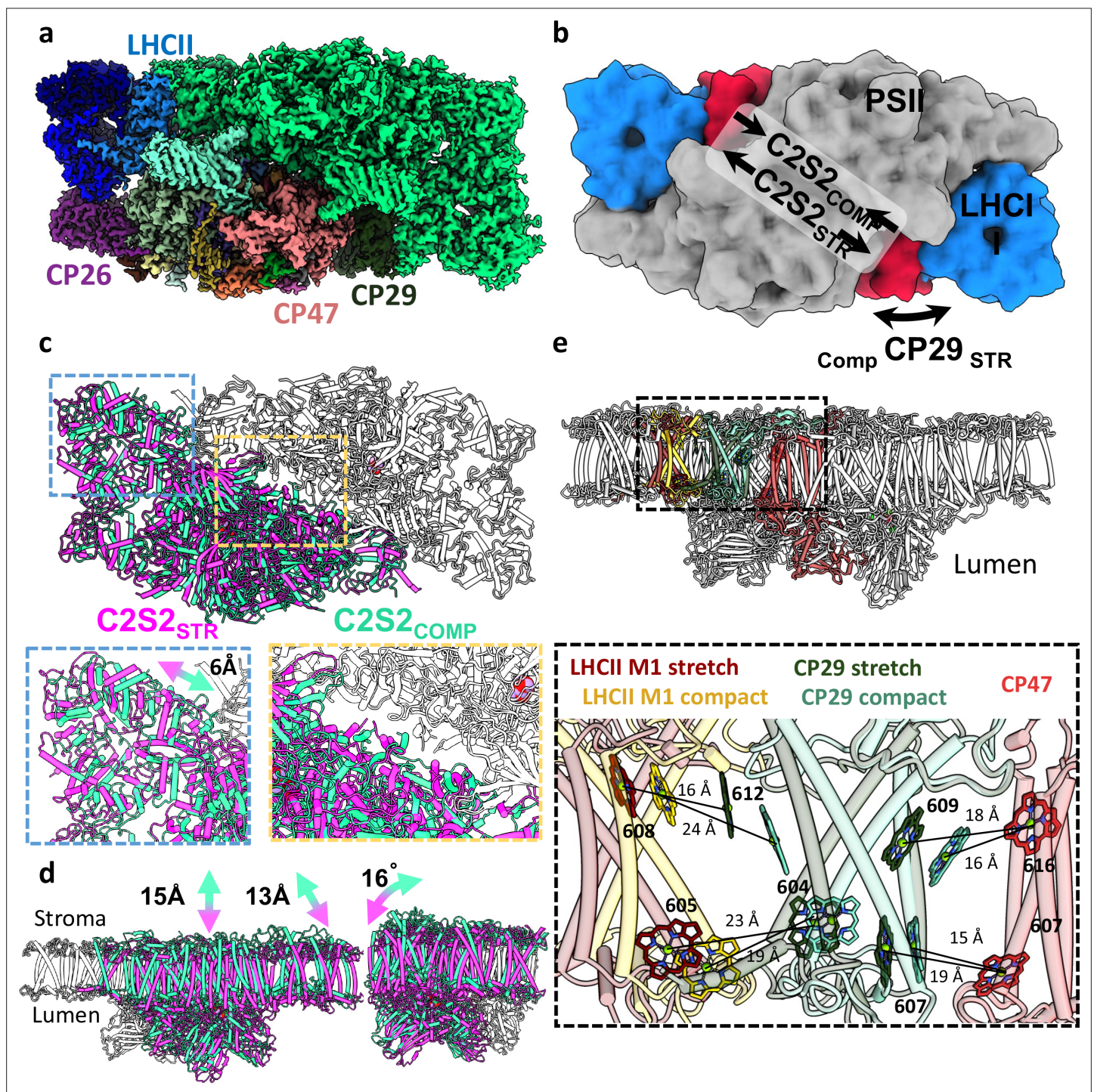


Figure 1. Two conformations of the eukaryotic photosystem II (PSII). **(a)** Overall view of the PSII C2S2 map in the compact conformation. One asymmetric unit is coloured in green, and in the other, each chain is coloured individually. PSII is shown from a luminal view in panels a–c. **(b)** Low-resolution model depicting the overall shifts in subunits between the two PSII conformations. CP29 in red, light-harvesting complex II (LHCII) in blue, and the two PSII cores in grey. **(c)** The two PSII conformations were superposed on one asymmetric unit (coloured in grey). The second asymmetric unit is coloured in magenta for the stretched conformation (C2S2_{STR}) and green for the compact conformation (C2S2_{COMP}). A close up showing a 6 Å shift in the position of LHCII and the lateral displacement between the two cores. **(d)** The stretched PSII conformation shows substantial drop in the membrane plane (13–15 Å, depending on the precise location), contributing to a larger inward curve (compared to the luminal space) of the entire supercomplex. Large deformations in the position of CP26 subunit which rotates by 16° between the two conformations. PSII is shown from a membrane plane view in panels d–e. **(e)** Considerable changes in the position of CP29 affect the transfer rates between LHCII and CP47. CP47 of both conformations (in red) is

Figure 1 continued on next page

Figure 1 continued

superposed, and distances between key chlorophylls (Chls) of CP29_{COMP} (light turquoise) and CP29_{STR} (dark green) show increased transfer distances in the stretched conformation. The distances between LHCII and CP29 follow an opposite trend, decreasing in the stretched conformation (LHCII_{STR} in dark red) and increasing in the compact conformation (LHCII_{COMP} in yellow). Distances were measured from the central manganese (Mg) atoms.

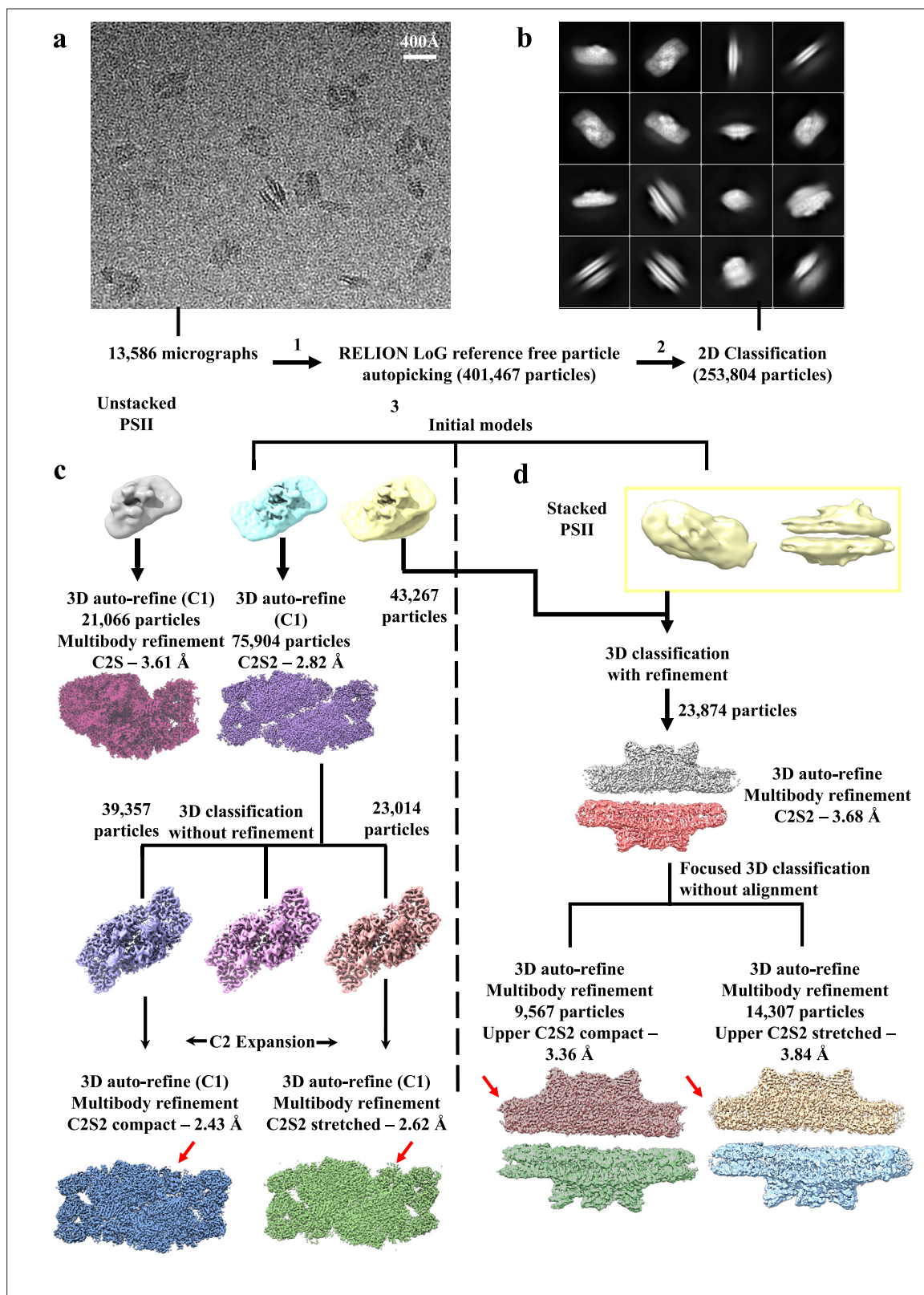


Figure 1—figure supplement 1. Cryo-EM data collection and processing scheme for unstacked and stacked photosystem II (PSII) complexes. (a) Sample micrograph collected for the *Dunaliella* PSII dataset displaying stacked and unstacked PSII particles from multiple views. (b) 2D classes showing stacked and unstacked PSII complexes. (c) Unstacked PSII data processing workflow after 2D classification. An Ab-initio model (coloured cyan) was created in RELION, followed by 3D classification and refinement, resulted in two distinct configuration – C2S (coloured brown-red) with a global Figure 1—figure supplement 1 continued on next page

Figure 1—figure supplement 1 continued

resolution of 3.61 Å, and C2S2 (coloured purple) with a global resolution of 2.82 Å. Next, 3D classification (without orientation refinement) was applied to the C2S2 set, and the dataset was separated to two conformations – C2S2 compact (coloured blue) with a global resolution of 2.43 Å, and C2S2 stretched (coloured green) with a global resolution of 2.62 Å. Red arrows show the different CP29 conformation. Particle numbers before C2 expansion are listed, see method section for full details. **(d)** Stacked PSII data processing workflow after 2D classification. An Ab-initio model (coloured yellow) was created in RELION, followed by 3D classification and refinement, resulting in a stacked PSII (coloured grey and red) with a global resolution of 3.68 Å. Next, focused 3D classification was applied on the stacked PSII, and the dataset was separated to two conformations according to the upper PSII dimer – stacked C2S2 compact (coloured chocolate and yellow-green) with a global resolution of 3.36 Å, and stacked C2S2 stretched (coloured wheat and sky-blue) with a global resolution of 3.84 Å. Red arrows show the difference between the compact and stretched conformations.

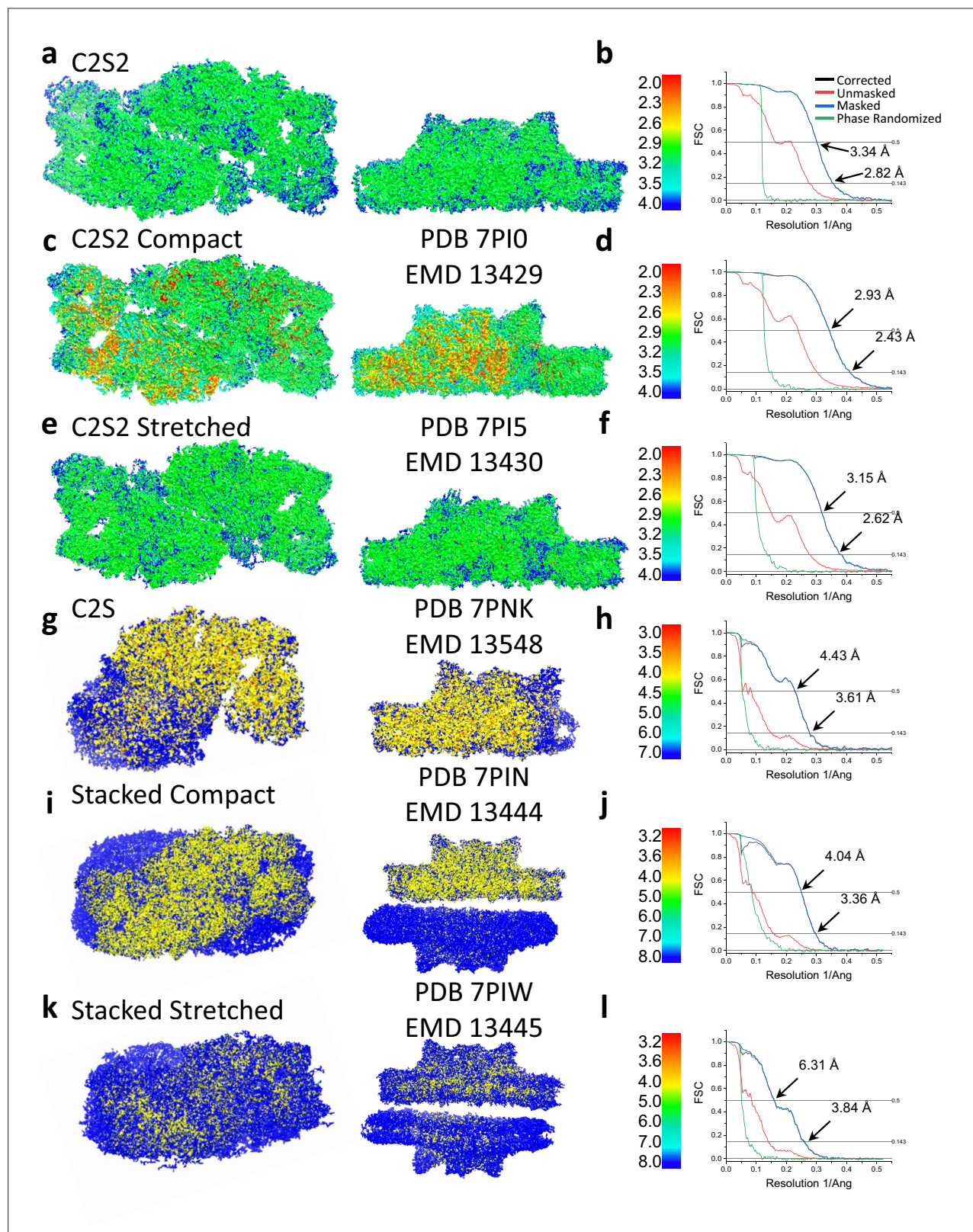


Figure 1—figure supplement 2. Local resolution and Fourier shell correlation (FSC) of *Dunaliella* photosystem II (PSII) supercomplexes. C2S2 local resolution (a) and FSC (b). C2S2 compact local resolution (c) and FSC (d). C2S2 stretched local resolution (e) and FSC (f). C2S local resolution (g) and FSC (h). Stacked C2S2 compact local resolution (i) and FSC (j). C2S2 local resolution (a) and FSC (b). Stacked C2S2 stretched local resolution (k) and FSC (l).

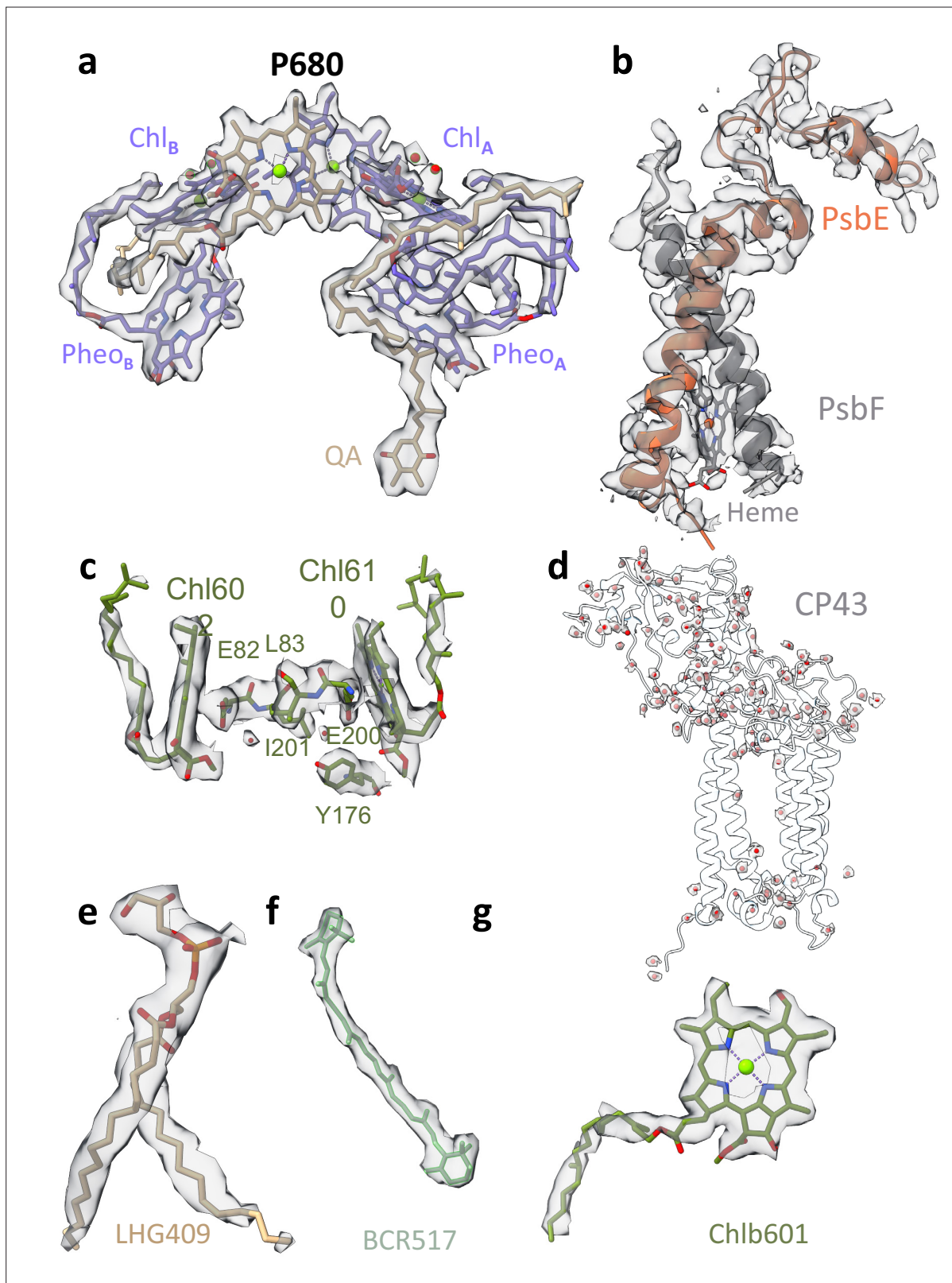


Figure 1—figure supplement 3. Map densities of unstacked *Dunaliella* photosystem II (PSII).

(a) PSII reaction centre chlorophylls (Chls), pheophytins, and quinone. Cryo-EM map shown in panels a–h at is contoured at 4 σ unless mentioned otherwise. (b) Cytochrome b559 heme, alpha, and beta subunits. (c) Light-harvesting complex II (LHCII) M2 Chls 602 and 610 alongside coordinating Glu82 and Glu200, Tyr176, Leu83, and Ile201. Water molecules located between a charged and hydrophobic amino acid are shown as red spheres.

Figure 1—figure supplement 3 continued on next page

Figure 1—figure supplement 3 continued

(d) Water molecules coordinated by the CP43 subunit shown as red spheres with their surrounding map. (e) D2 1,2-dipalmitoyl-phosphatidyl-glycerole 409. (f) CP43 β -carotene 517. (g) LHCII M2 Chl b 601. Map shown in 3.5σ contour.

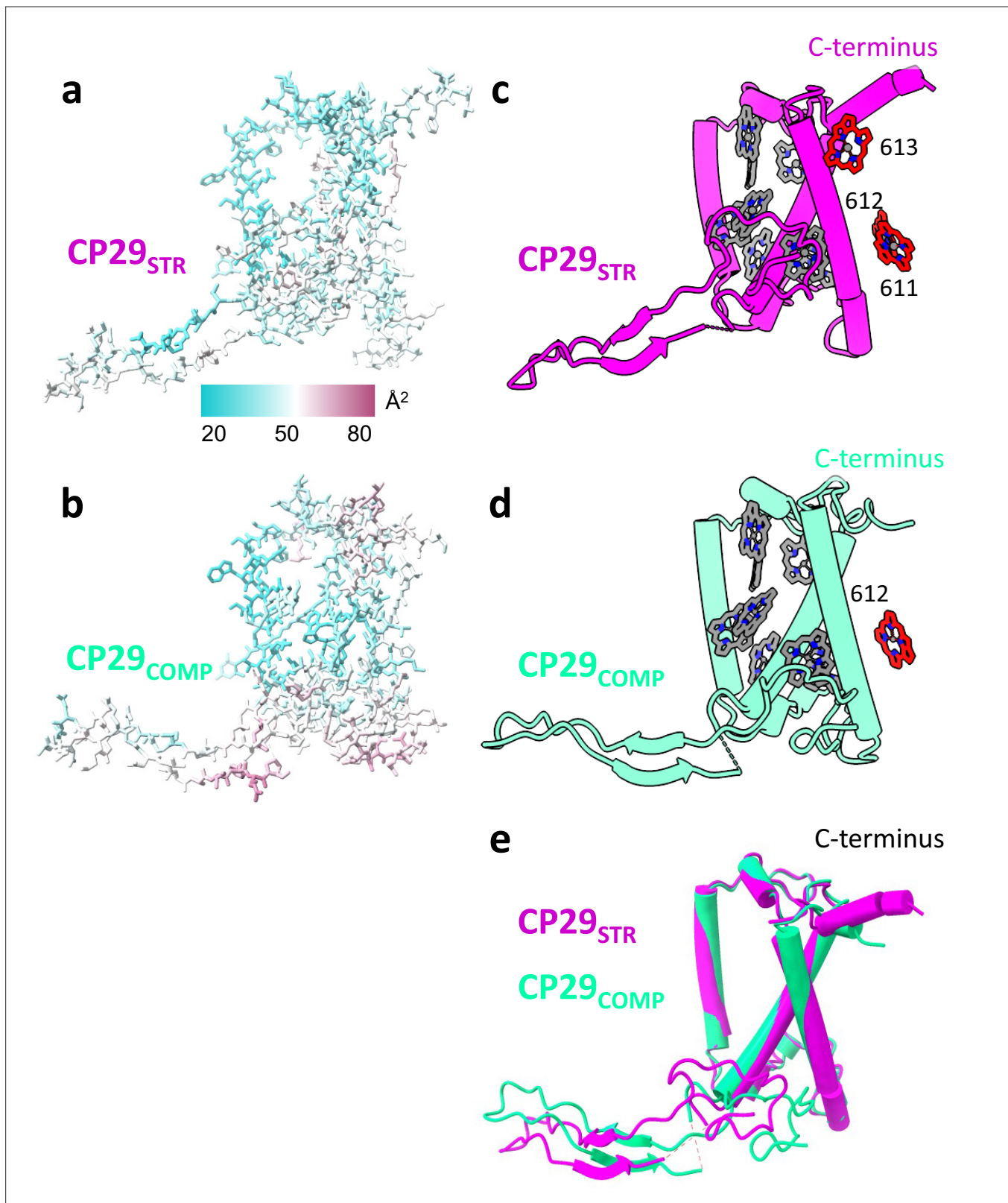


Figure 1—figure supplement 4. Comparing CP29_{STR} and CP29_{COMP}. (a and b) CP29_{STR} and CP29_{COMP} backbone, side chains and carotenes, coloured according to their b-factor values, displaying a similar distribution of b-factors in both conformations. (c and d) CP29_{STR} and CP29_{COMP} showing chlorophyll (Chl) differences between the two structures (Chl 611 and 613 missing in CP29_{COMP}). (e) Superposition of CP29_{STR} and CP29_{COMP} showing that overall, the structures are similar. The two structures were superposed along their trans-membrane helices which leads to positional shifts in their

Figure 1—figure supplement 4 continued on next page

Figure 1—figure supplement 4 continued

N-terminal loop. Within photosystem II (PSII) the N-terminal loop binds to the same site on the PSII core (mostly CP47) while the core of CP29 is rotated (**Figure 1—figure supplement 5**). The structure of the C-terminus is disturbed in CP29_{COMP}.

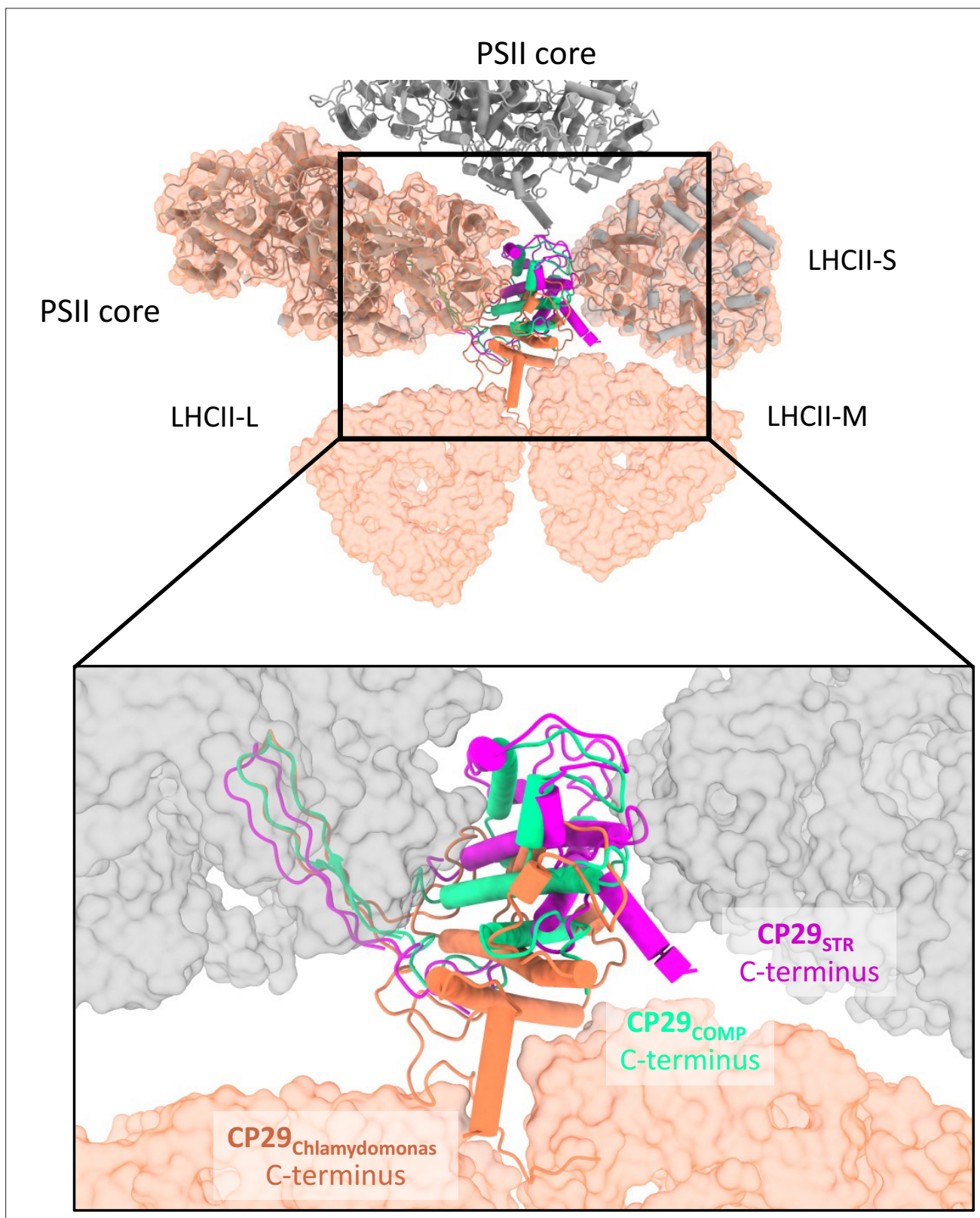


Figure 1—figure supplement 5. Comparing CP29 positions between *Dunaliella* and *Chlamydomonas reinhardtii* (Cr). Photosystem II (PSII) from Cr is shown as a molecular surface coloured orange and was superposed on PSII_{COMP} and PSII_{STR} using the core subunits (grey tubes). The different orientations of CP29 are clearly visible, with the position of CP29_{COMP} as a possible intermediate between C₂S₂ and C₂S₂M₂L₂. The orientation and folding of the C-terminus seems to be associated with light-harvesting complex II (LHCII) binding.

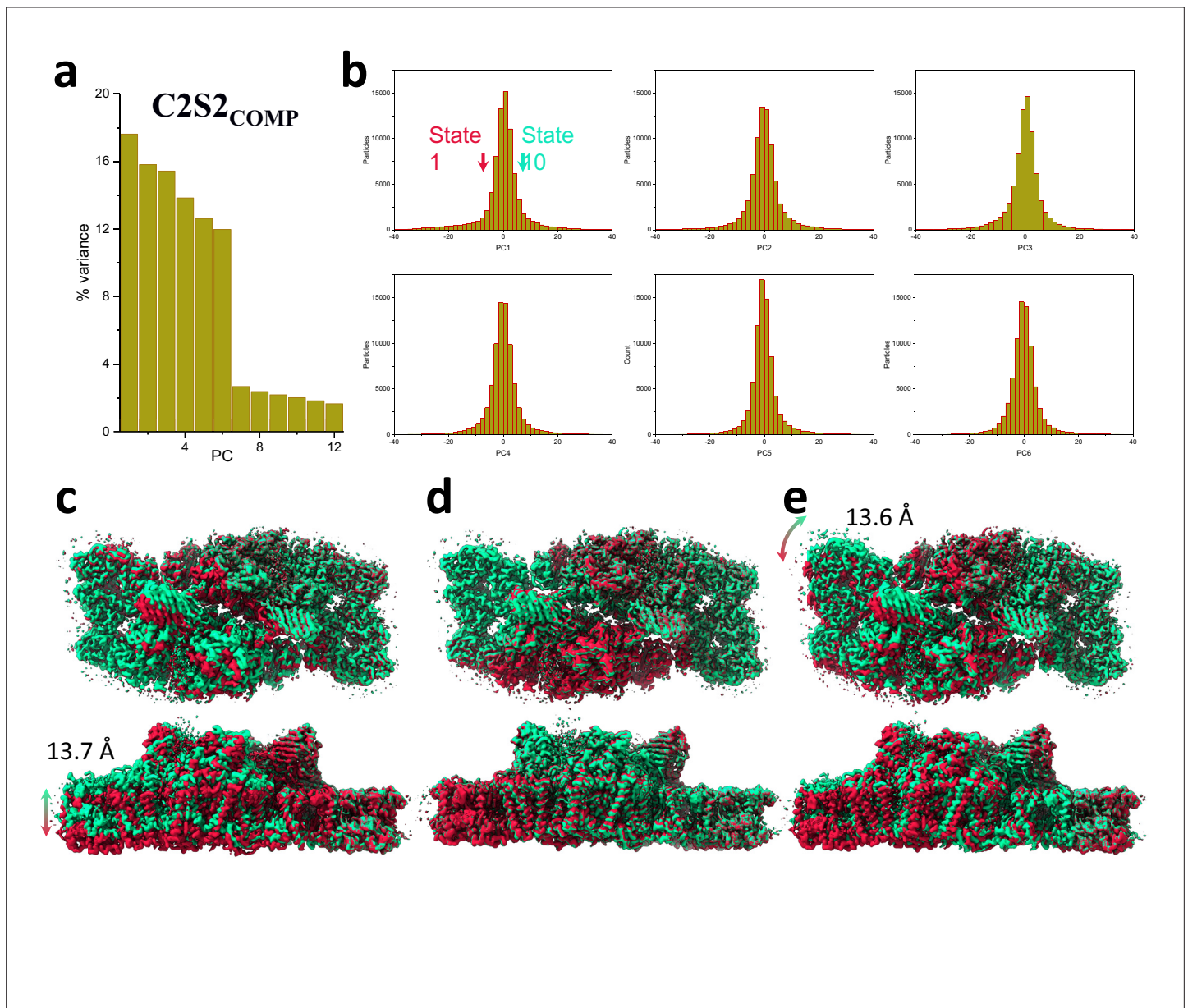


Figure 1—figure supplement 6. Principal component (PC) analysis of C2S2_{COMP}.

(a) Percent of the variance explained by each of the 12 PCs. (b) The particle distribution along the first six PCs shows continuous heterogeneity in the C2S2_{COMP}. States 1 and 10 are marked with a red and green arrow, respectively. (c) To visualize the state differences, one photosystem II (PSII) monomer was superposed, and the other monomer was used to visualize the differences. Luminal view (top), membrane plane view along the long axis (middle), and short axis (bottom) show the shift in position of C2S2_{COMP} in the first PC. (d) Luminal view (top), membrane plane view along the long axis (middle), and short axis (bottom) show the shift in position of C2S2_{COMP} in the second PC. (e) Luminal view (top), membrane plane view along the long axis (middle), and short axis (bottom) show the shift in position of C2S2_{COMP} in the third PC.

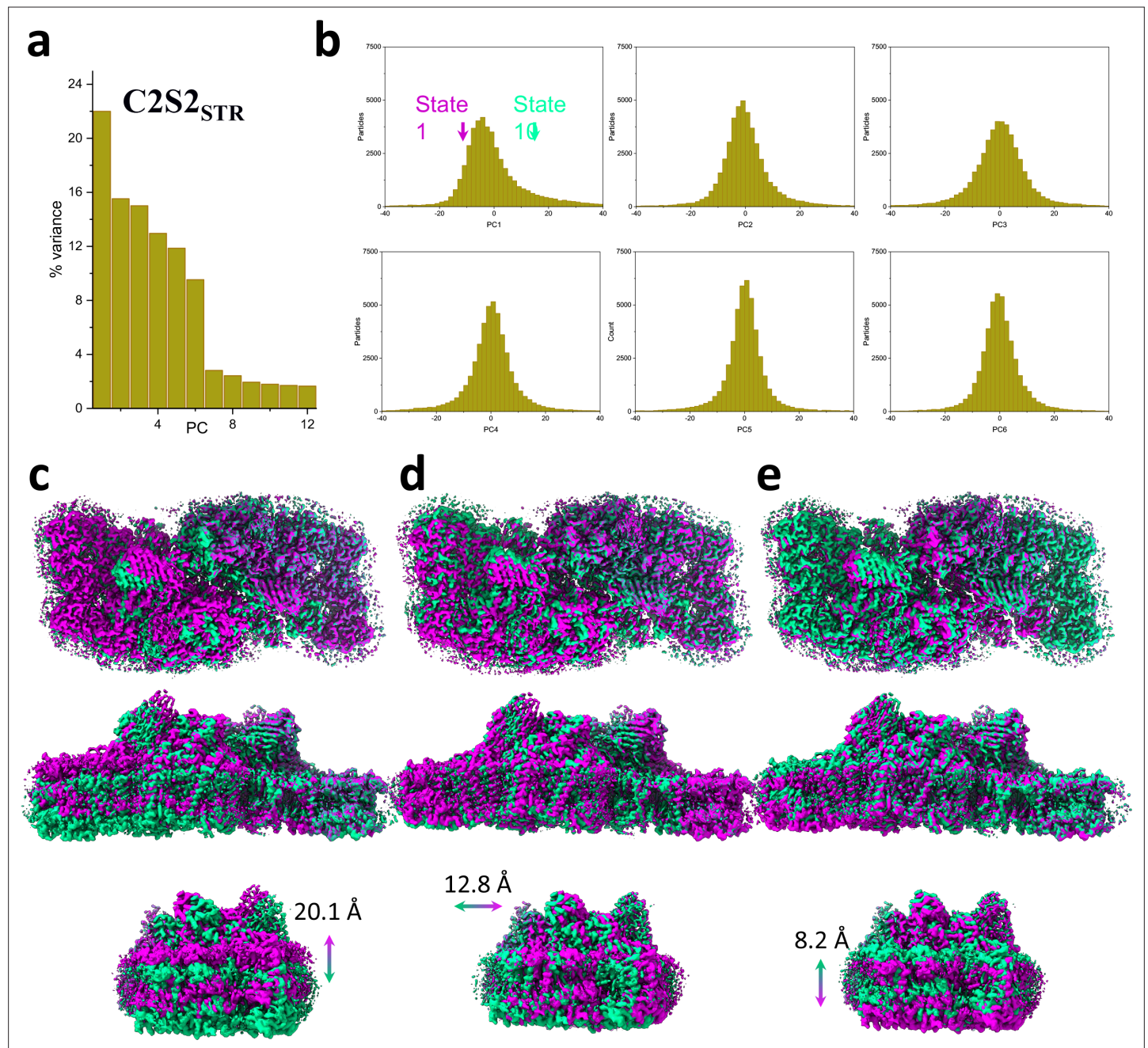


Figure 1—figure supplement 7. Principal component (PC) analysis of C2S2_{STR}.

(a) Percent of the variance explained by each of the 12 PCs. (b) The particle distribution along the first six PCs shows continuous heterogeneity in the C2S2_{STR}. States 1 and 10 are marked with a magenta and teal arrow, respectively. (c) Luminal view (top), membrane plane view along the long axis (middle), and short axis (bottom) show the shift in position of C2S2_{STR} in the first PC. (d) Luminal view (top), membrane plane view along the long axis (middle), and short axis (bottom) show the shift in position of C2S2_{STR} in the second PC. (e) Luminal view (top), membrane plane view along the long axis (middle), and short axis (bottom) show the shift in position of C2S2_{STR} in the third PC.

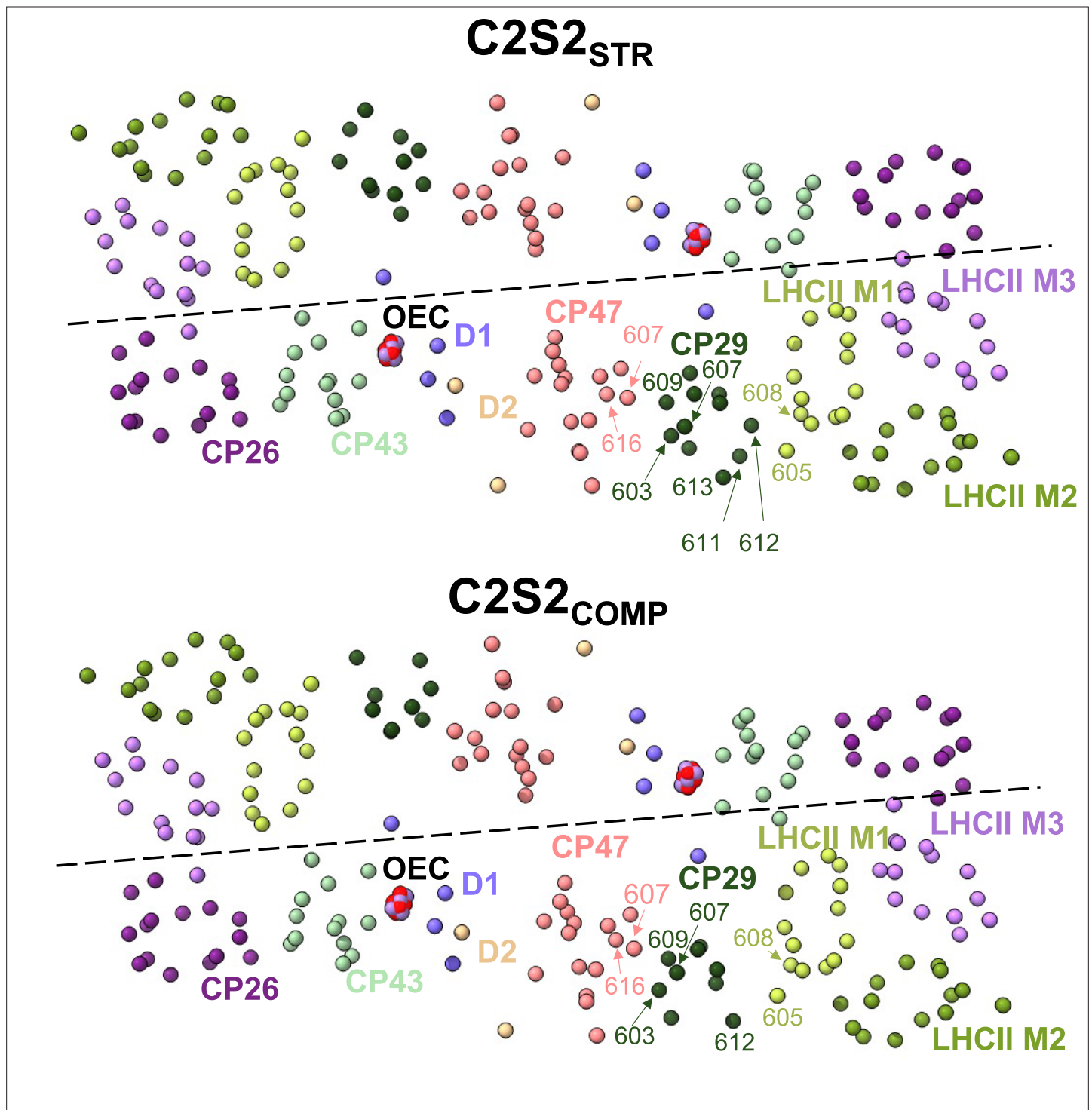


Figure 1—figure supplement 8. Changes in CP29 chlorophyll (Chl) positions between C2S2_{COMP} and C2S2_{STR}. Several CP29 Chl molecules in C2S2_{STR} are positioned close to light-harvesting complex II (LHCII) and can mediate faster excitation energy transfer (EET) from LHCII to photosystem II (PSII), whereas in C2S2_{COMP} CP29 is positioned closer to CP47 and moves away from LHCII. In the C2S2_{STR} conformation, CP29 stromal Chl 612 and Chl 611 are located 16 and 22 Å, respectively, from LHCII M1 Chl 608, while CP29 luminal Chl 613 is located 20 Å from LHCII M1 Chl 605, and CP29 Chl 604 is positioned 23 Å from both LHCII M1 Chl 604 and Chl b 605 (**Figure 1e**). On the opposite end of CP29, stromal Chl 609 and Chl 603 are found 18 and 22 Å, respectively, from CP47 Chl 616, while luminal Chl b 607 is found 19 Å from CP47 Chl 607. C2S2_{COMP} presents an opposite connectivity – CP29 Chl 612 is located 24 Å from LHCII M1 Chl 608, and CP29 Chl 604 is located 19 and 23 Å from LHCII M1 Chl b 605 and Chl 604, respectively. On the other hand, the rotation of CP29 into the monomer-monomer interface in C2S2_{COMP} set CP29 Chl 603 and Chl 609 19 and 16 Å, respectively, from CP47 Chl 616, while CP29 Chl b 607 is located 15 Å from CP47 Chl 607 (**Figure 1e**). Chls are presented as spheres, coloured according to their subunit, and the oxygen-evolving complex (OEC) is shown in red and purple sphere.

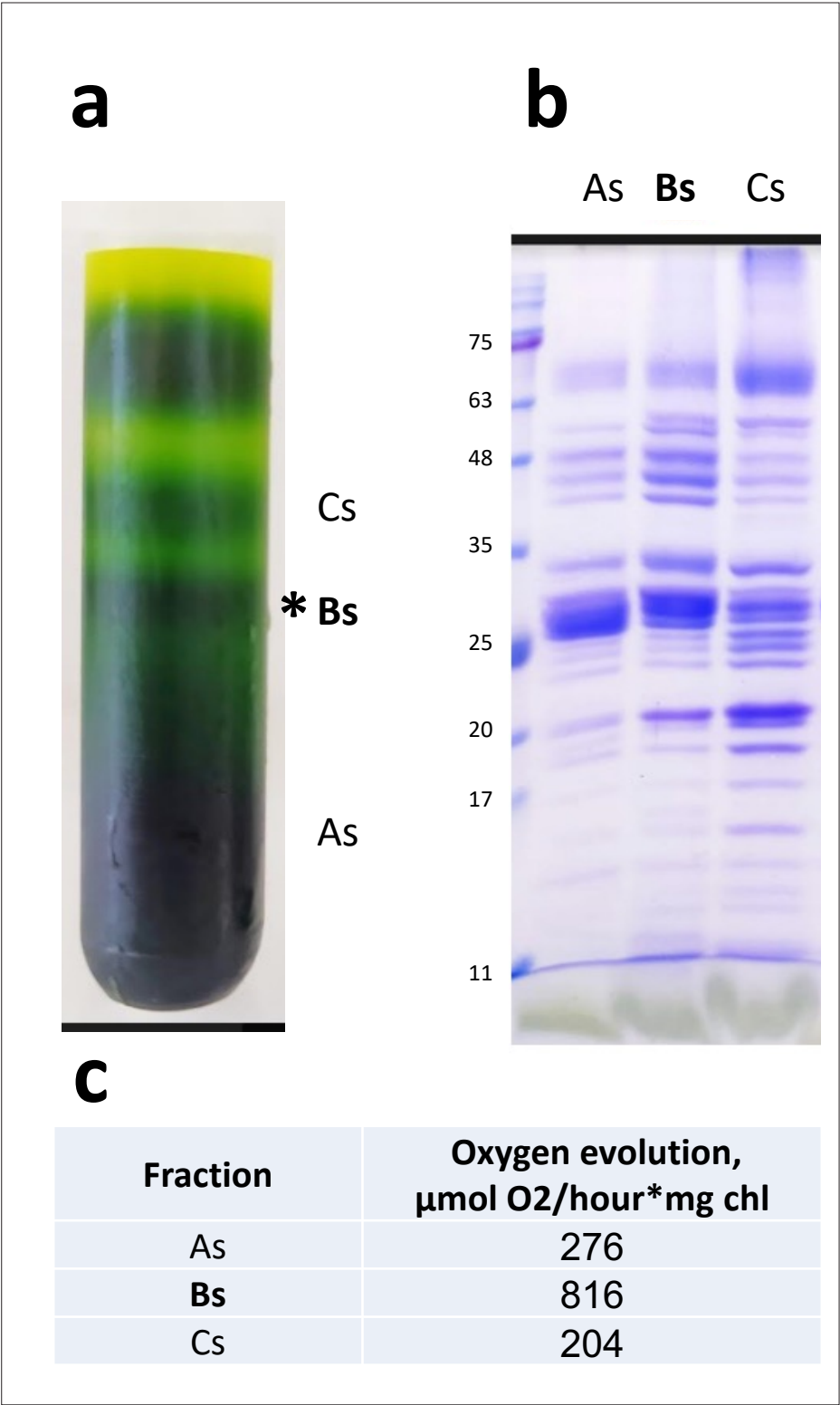


Figure 1—figure supplement 9. Sucrose gradient and sodium dodecyl sulfate–polyacrylamide gel electrophoresis (SDS-PAGE) of *Dunaliella* photosystem II (PSII) preparation. **(a)** Sucrose density gradient of the final *Dunaliella* PSII preparation. The three fractions collected are marked As, Bs, and Cs. The Bs fraction was used for cryo-EM data collection. **(b)** SDS-PAGE of the three fractions. **(c)** Oxygen evolution rates for the collected fractions.

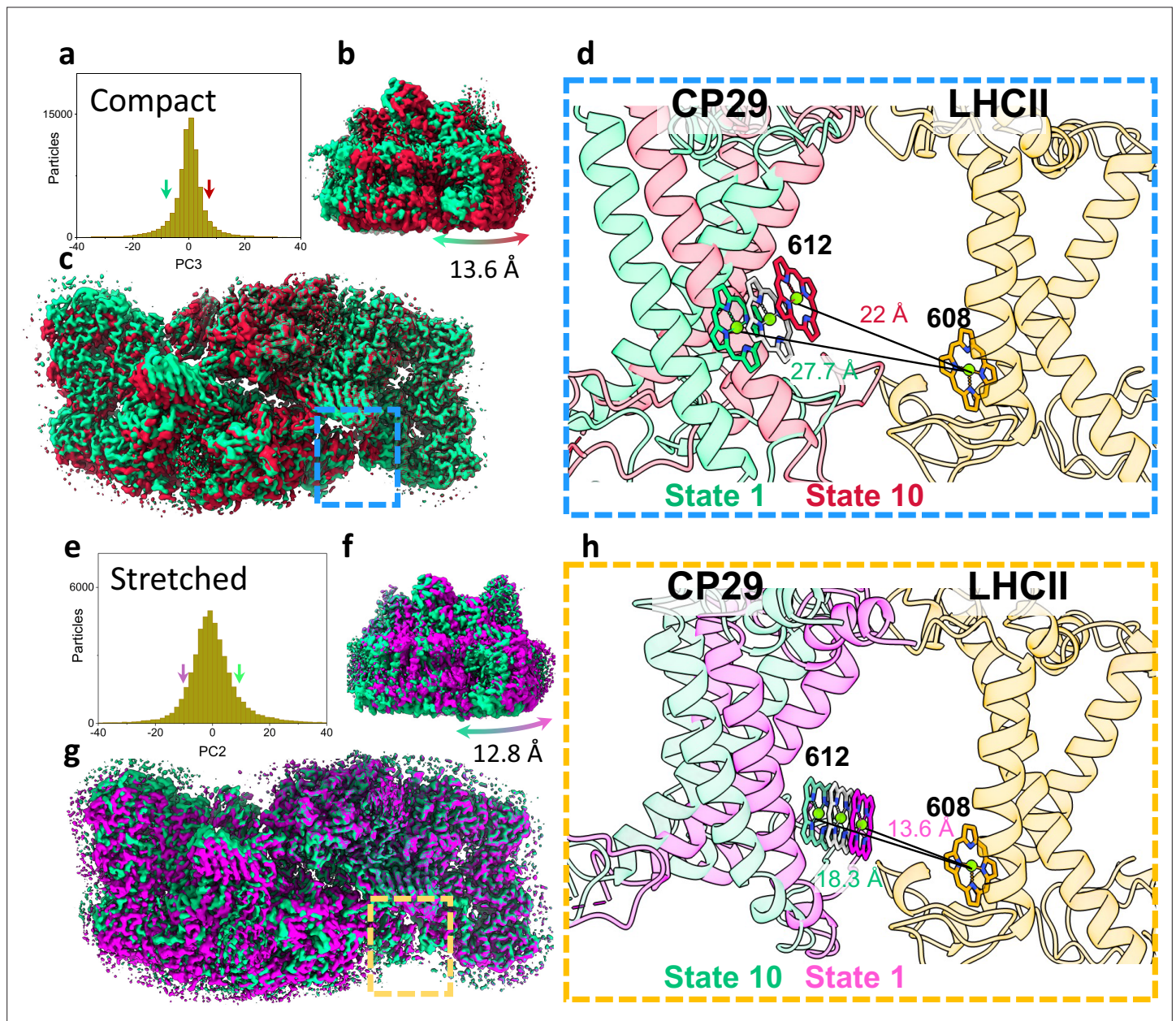


Figure 2. Heterogeneity within photosystem II (PSII) states.

(a) Continuous heterogeneity of C2S2_{COMP} particles distribution along the third principal component (PC) axis. Each PC was divided into 10 states separated by 9% of the particle population along the PC axis. State 1 (corresponding to the position of the ninth percentile on the PC axis) is marked with a green arrow and state 10 (corresponding to the position of the 91st percentile on the PC axis) with a red arrow. States 1 and 10 are coloured in green and red in panels a–d. (b) To maximize the state differences on the left monomer, the maps were superposed along the region of the right PSII monomer. Membrane plane view of the shift in position of C2S2_{COMP} in the third PC. (c) Luminal view of the shift in position of C2S2_{COMP}. CP29 and light-harvesting complex II (LHCII) are marked with a blue rectangle (d) Zoom-in on the change in CP29 position between states 1 and 10. The change in distance between CP29 Chl 612 and LHCII M1 Chl 608 is shown. LHCII M1 (from the superposed PSII monomer) is coloured light orange, and the consensus position of Chl 612 is shown in grey. (e) Continuous heterogeneity of C2S2_{STR} particles distribution in the second PC. State 1 is marked with a magenta arrow and state 10 with a teal arrow. Colours are maintained in panels e–h. (f) Membrane plane view of the shift in position of C2S2_{STR}. CP29 and LHCII are marked with an orange rectangle. (g) Luminal view of the shift in position of C2S2_{STR}. CP29 and LHCII are marked with an orange rectangle. (h) Zoom-in on the change in CP29 position between states 1 and 10. The change in distance between CP29 Chl 612 and LHCII M1 Chl 608 is shown. LHCII M1 is coloured orange, and the consensus position of Chl 612 is shown in grey.

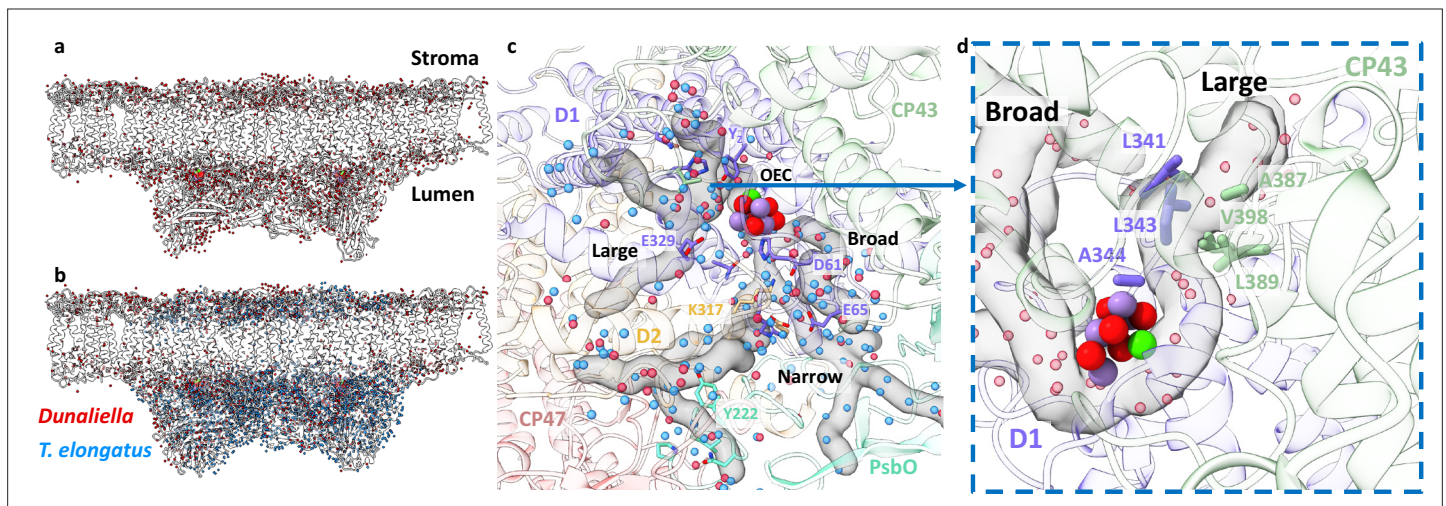


Figure 3. Water distribution and channels in eukaryotic photosystem II (PSII).

(a) Water molecules distribution in *Dunaliella* C2S2_{COMP} structure. The protein scaffold is coloured grey, and water molecules are shown as red spheres. (b) Water molecules distribution in *Dunaliella* C2S2_{COMP} compared to *Thermosynechococcus elongatus* PSII core (PDBID 3WU2). *T. elongatus* water molecules are shown as blue spheres. (c) *Dunaliella* PSII water channels identified by CAVER analysis, shown as grey transparent maps. The Large, Narrow, and Broad channels are annotated along with selected amino acids coloured according to their respective subunits. Water molecules are presented as in panel b. (d) A hydrophobic patch identified in the large channel near the oxygen-evolving complex (OEC), which may serve as an O₂ release pathway. The region shown is indicated by the blue arrow, but the orientation is different to improve visualisation.

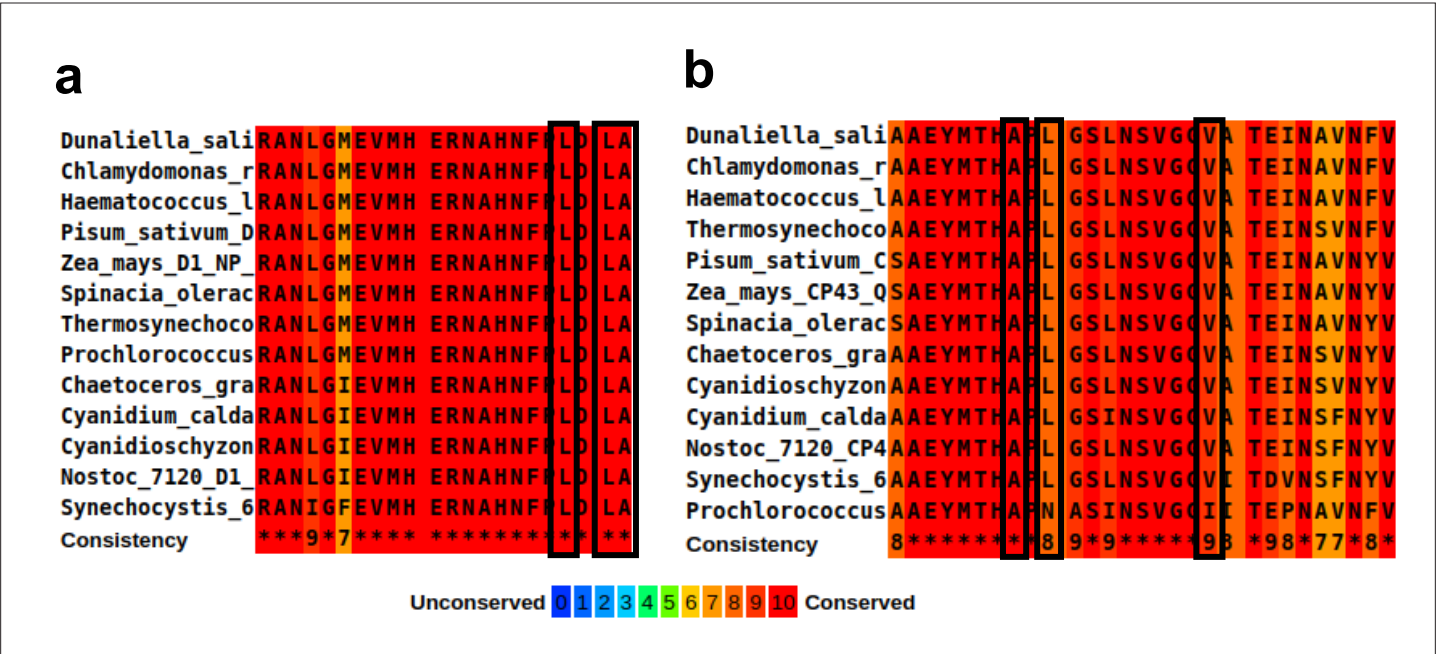


Figure 3—figure supplement 1. Sequence alignment of the hydrophobic residues lining the large channel cavity near oxygen-evolving complex (OEC). (a) Alignment of D1 C-terminus domain, residues 323–344. The hydrophobic residues are marked with black rectangles, together with their conservation score. The organisms used for alignment in panels a and b are *Synechocystis* sp. PCC 6803, *Thermosynechococcus elongatus*, *Nostoc* sp. PCC 7120, *Prochlorococcus marinus*, *Cyanidium caldarium*, *Cyanidischyzon merolae*, *Chaetoceros gracilis*, *Dunaliella salina*, *Chlamydomonas reinhardtii*, *Haematococcus lacustris*, *Pisum sativum*, *Zea mays*, and *Spinacia oleracea*. (b) Alignment of CP43 residues 380–408. The hydrophobic residues are marked with black rectangles, together with their conservation score.

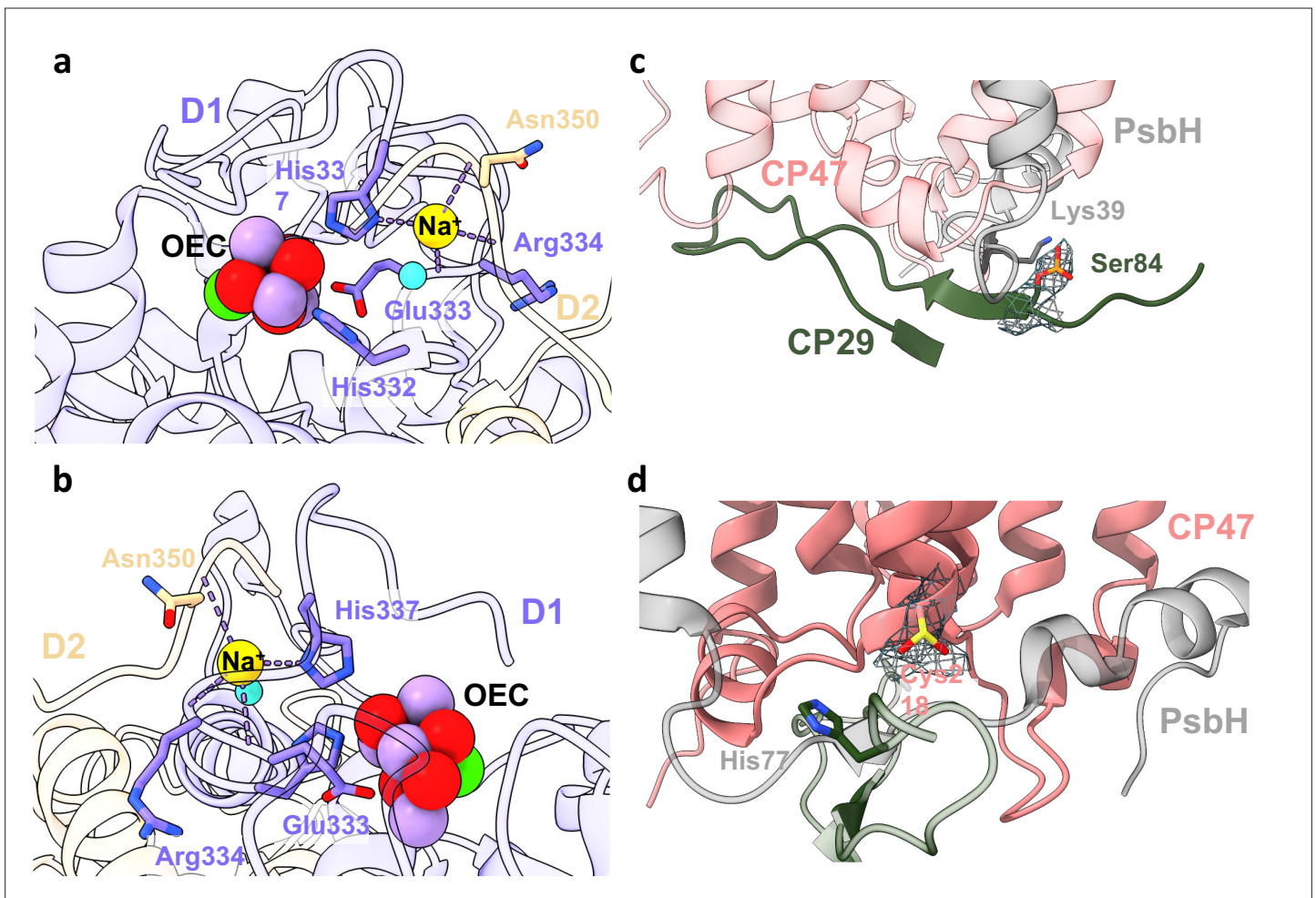


Figure 3—figure supplement 2. Na⁺ ion and post-translational modifications (PTMs) in *Dunaliella* photosystem II (PSII).

(a) Na⁺ binding site close to the oxygen-evolving complex (OEC). The Na⁺ ion is coordinated by D1 histidine 337, the backbone carbonyls of D1 glutamic acid 333, arginine 334, D2 asparagine 350, and a water molecule. Amino acids are coloured according to their respective subunits, water molecule as a turquoise sphere, and the OEC coloured red, purple, and green. (b) Rotated view of Na⁺ binding site. (c) CP29 phosphorylated serine 84 and adjacent subunits at the stromal interface. Map surrounding the phosphorylated serine is shown at 3.5σ contour. PsbH lysine 39 coordinating the phosphate is coloured grey, CP29 N-terminal region in dark-green, and CP47 in coral. (d) CP47 sulfenylated cysteine 218 at the stromal region, along with map density at 4σ contour. PsbH histidine 77 coloured grey and CP47 in coral.

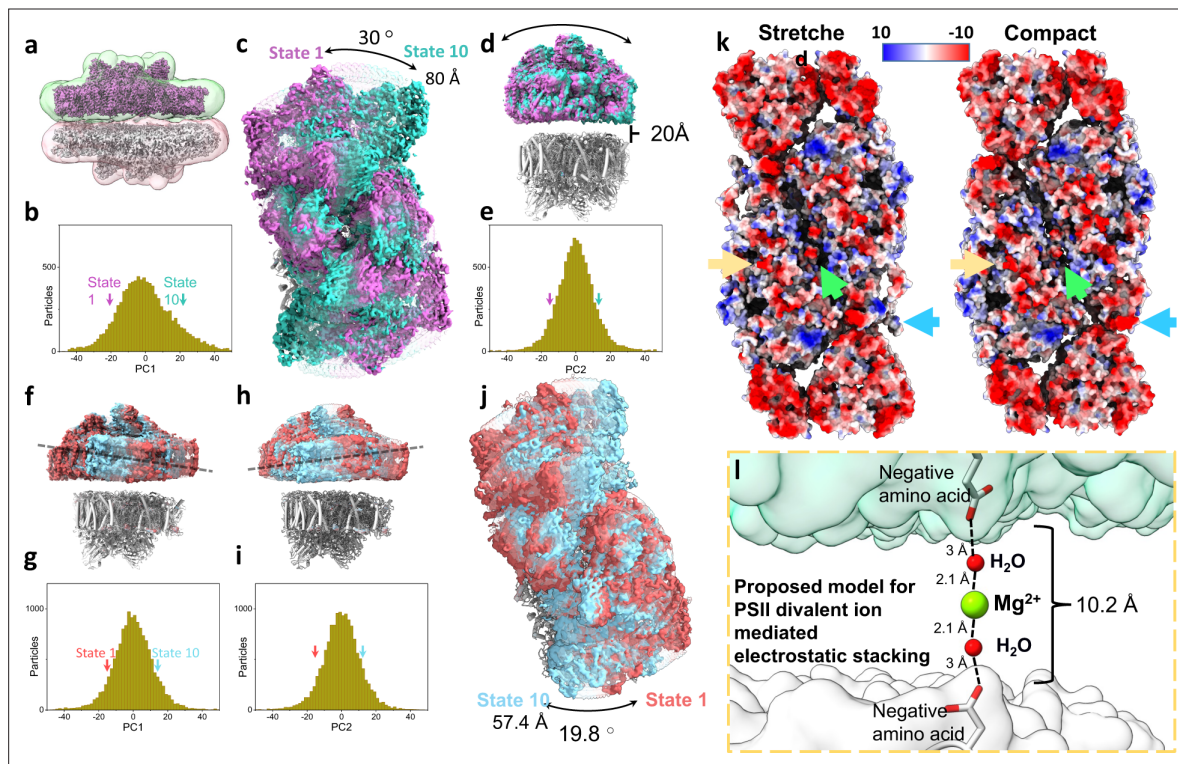


Figure 4. Heterogeneity, electrostatic interactions, and model for photosystem II (PSII) stacking.

(a) Stacked *Dunaliella* PSII C2S2_{COMP} maps, and the masks used for multibody refinement. Maps are coloured magenta and grey and masks in green and red. (b) The particle distribution along the first principal component (PC) shows continuous heterogeneity in the stacked C2S2_{COMP}. State 1 is marked with a magenta arrow and state 10 with a teal arrow (colours are preserved in panels b–e). (c) Luminal view of the rotation of the upper PSII dimer between state 1 and state 10 (the bottom dimer was kept in a fixed position). (d) Membrane plane view of the shift in position of the upper PSII dimer in C2S2_{COMP} second PC. The distance between the upper and lower PSII is shown. (e) Particle distribution along the second PC of the stacked C2S2_{COMP} shows continuous heterogeneity. (f) Membrane plane view of the tilt in the upper PSII dimer in C2S2_{STR} particle set first PC. The direction of the tilt is marked with a dashed line. State 1 is coloured red and state 10 in cyan (colours are preserved in panels f–j). (g) Continuous heterogeneity in the stacked C2S2_{STR} particles distribution along the first PC. (h) Membrane plane view of the tilt in orientation of the upper PSII dimer in C2S2_{STR} second PC (with the bottom dimer kept fixed). The dashed line shows the tilt axis is opposite to that shown in panel f. (i) Continuous heterogeneity of stacked C2S2_{STR} particles distribution in the second PC. (j) Luminal view of the rotation of the upper PSII dimer between state 1 and state 10. (k) Coulombic electrostatic potential of the stromal region of the stretched (left) and compact (right) conformations. Differences are marked for CP47 C-terminus (orange arrow), the intermonomer space (green arrow) and CP29 (blue arrow). The negative potentials ($0 \text{ } k_B T/e < \Phi < -10 \text{ } k_B T/e$) are coloured red, and the positive potentials ($0 \text{ } k_B T/e < \Phi < 10 \text{ } k_B T/e$) are coloured blue. (l) Proposed hypothetical model for PSII stacking mediated by negatively charged amino acids and Mg²⁺ ions (density for Mg²⁺ ions is not observed in our map). Upper PSII shown as a green surface and the lower PSII as a white surface.

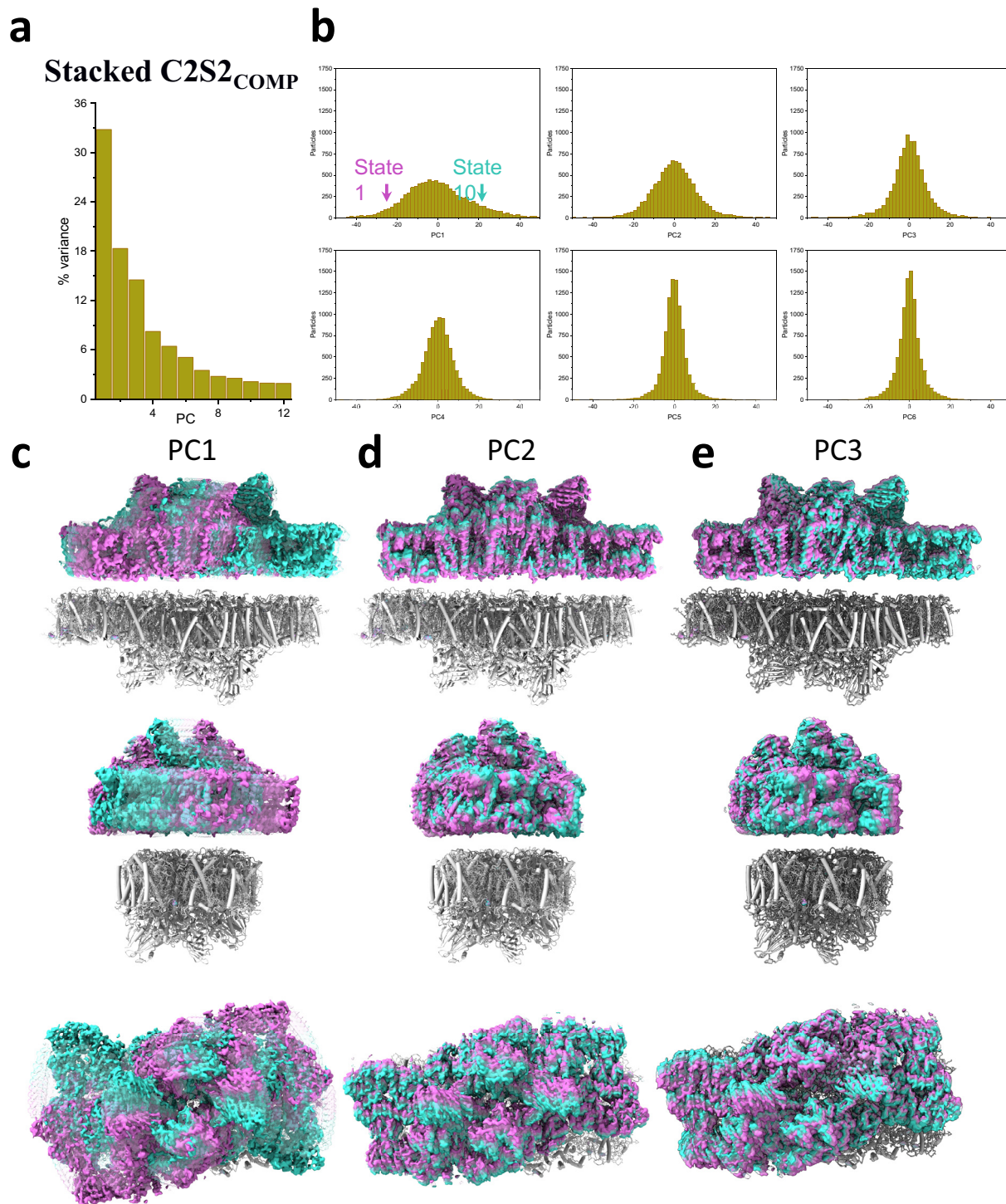


Figure 4—figure supplement 1. Principal component (PC) analysis of stacked C2S2_{COMP}.

(a) Percent of the variance explained by each of the 12 PCs. (b) The particle distribution along the first six PCs shows continuous heterogeneity in the C2S2_{COMP}. States 1 and 10 are marked with a magenta and teal arrow, respectively. (c) Membrane plane view along the long axis (top), the short axis (middle), and luminal view (bottom) show the shift in position of stacked C2S2_{COMP} in the first PC. (d) Membrane plane view along the long axis (top), the

Figure 4—figure supplement 1 continued on next page

Figure 4—figure supplement 1 continued

short axis (middle), and luminal view (bottom) show the shift in position of stacked C2S2_{COMP} in the second PC. **(e)** Membrane plane view along the long axis (top), the short axis (middle), and luminal view (bottom) show the shift in position of stacked C2S2_{COMP} in the third PC.

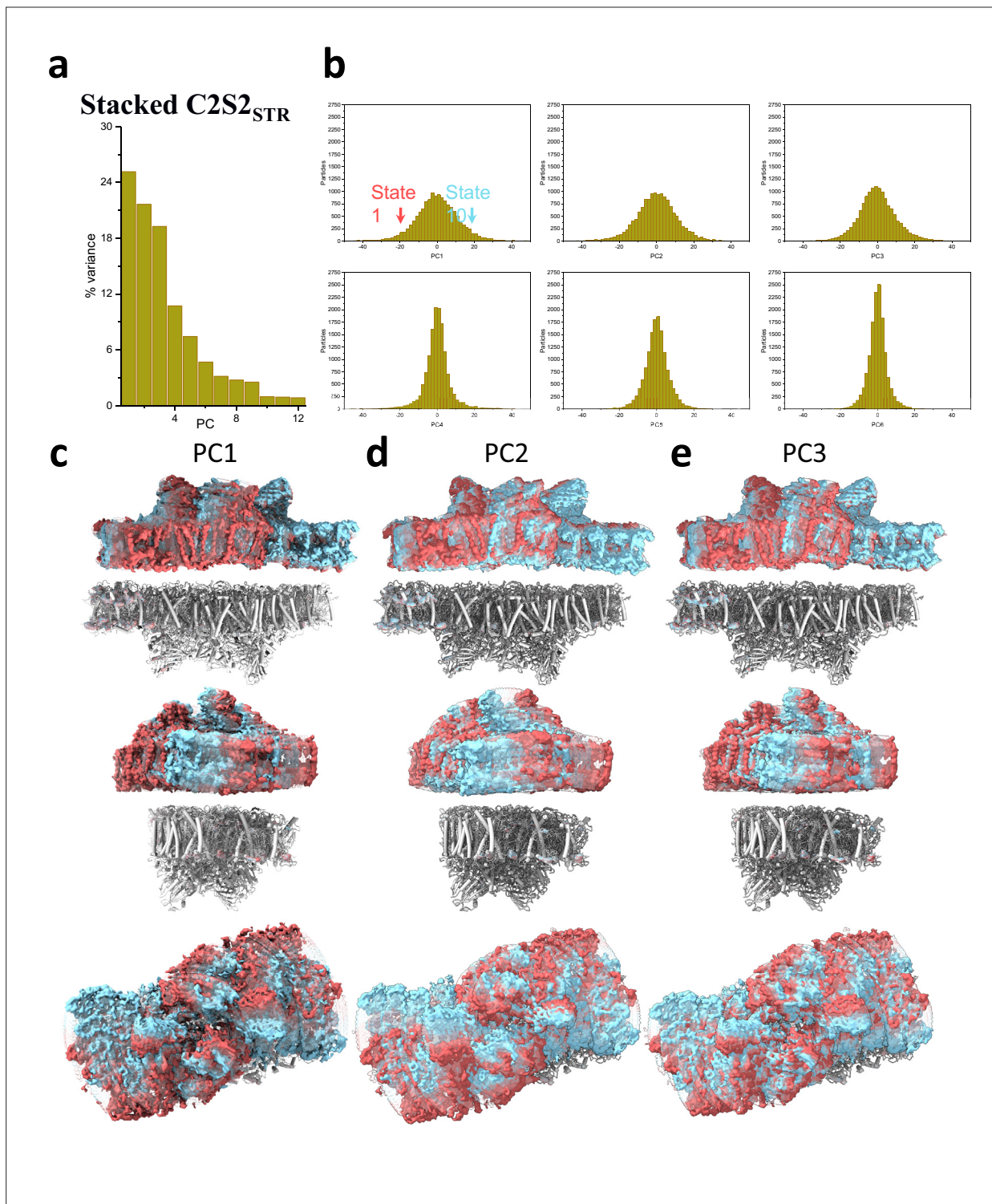


Figure 4—figure supplement 2. Principal component (PC) analysis of stacked C2S2_{STR}.

(a) Percent of the variance explained by each of the 12 PCs. (b) The particle distribution along the first six PCs shows continuous heterogeneity in the C2S2_{STR}. States 1 and 10 are marked with a red and cyan arrow, respectively. (c) Membrane plane view along the long axis (top), the short axis (middle), and luminal view (bottom) show the shift in position of stacked C2S2_{STR} in the first PC. (d) Membrane plane view along the long axis (top), the short axis (middle), and luminal view (bottom) show the shift in position of stacked C2S2_{STR} in the second PC. (e) Membrane plane view along the long axis (top), the short axis (middle), and luminal view (bottom) show the shift in position of stacked C2S2_{STR} in the third PC.

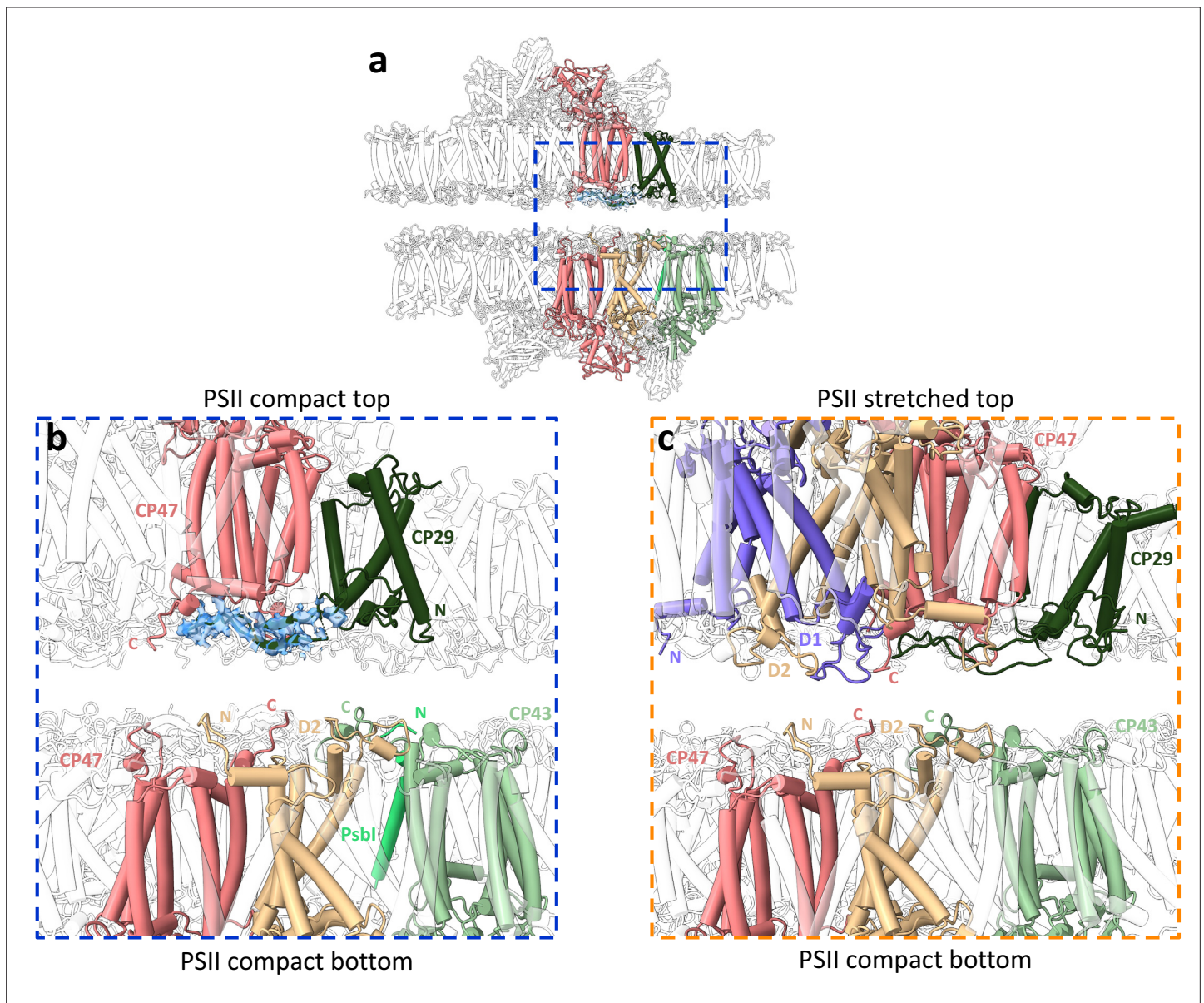


Figure 4—figure supplement 3. Stromal interactions between photosystem II (PSII) subunits in the stacked configurations.

(a) Structure of stacked *Dunaliella* C2S2_{COMP} showing a shift in position of each PSII dimer. The region where PSII core subunits are nearest is marked with a blue rectangle. (b) Zoom-in on the stromal interactions between PSII_{COMP} dimers, displaying close subunits from both dimers. The map density near CP29 is shown at 2σ , coloured in transparent blue. Subunits are colour coded, and the C- and N-termini are marked as C and N, respectively. (c) Zoom-in on the stromal interactions between PSII_{STR} dimers, displaying close subunits from both dimers.

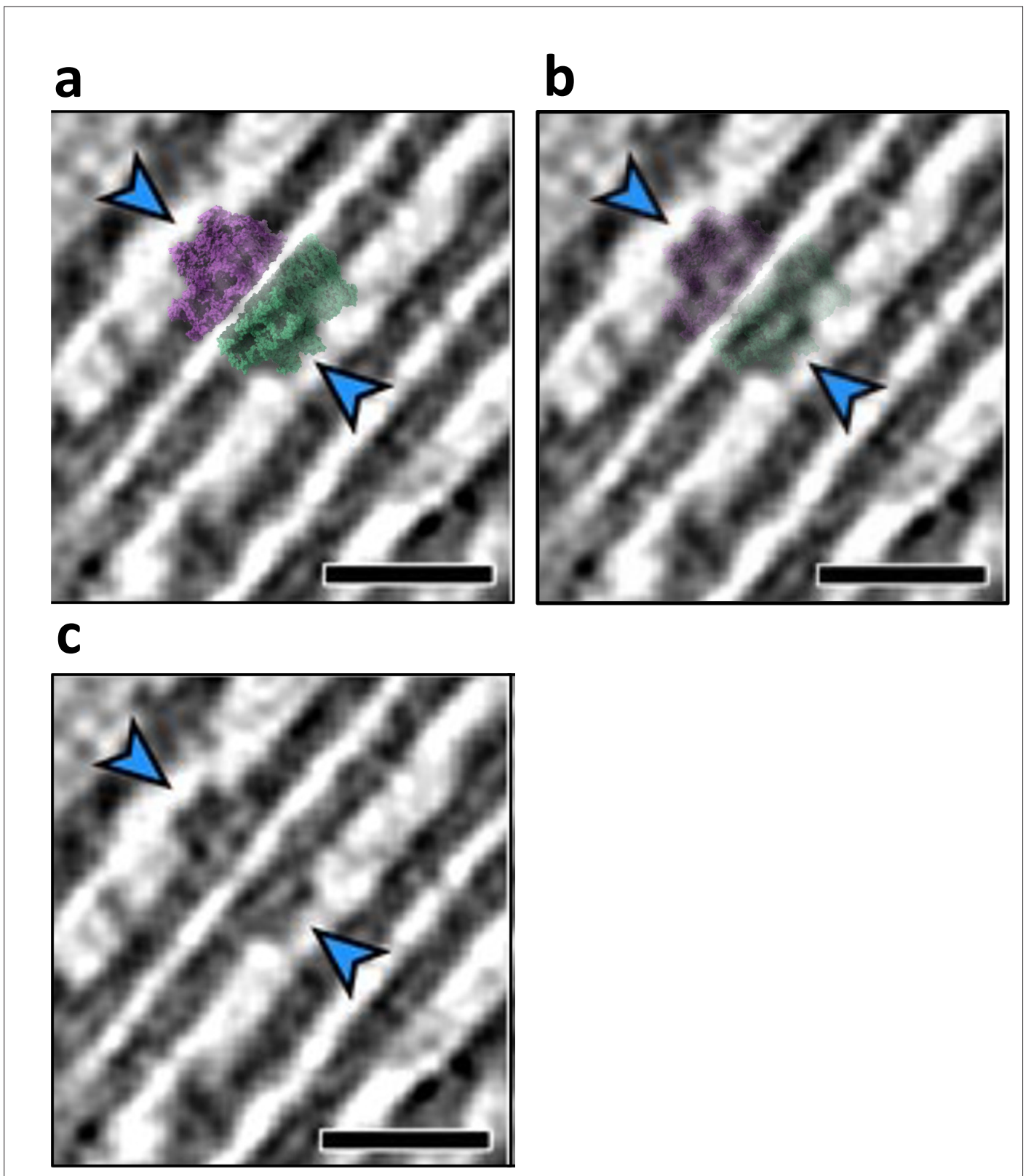


Figure 4—figure supplement 4. Similar membrane separation in purified and in-vivo detected stacked photosystem II (PSII) complexes. Panels **a**, **b**, and **c** show **Figure 1D** from Wietrzynski et al. showing appressed thylakoid membranes in a native state. The stacked PSII dimer (PDBID 7PIN) was back-projected onto the tomogram and is shown at two different transparencies (**a** and **b**). Panel **c** is the original, unmodified figure. Scale bar 20 nm.

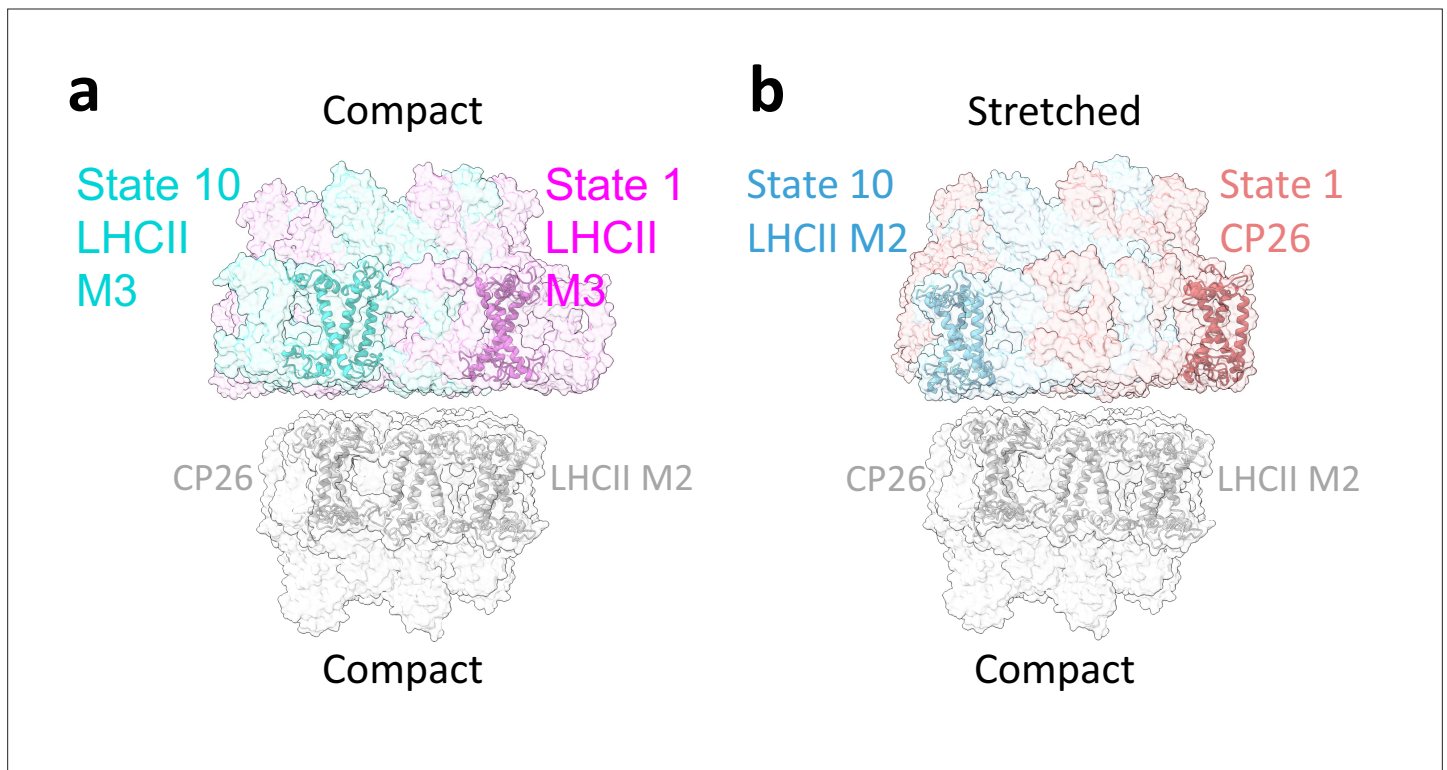


Figure 4—figure supplement 5. Light-harvesting complex (LHC) interactions limit stacked photosystem II (PSII) rotation. **(a)** In stacked $C2S2_{COMP}$ (right), the rotation is confined by LHCII M3 in state 1 (magenta) and 10 (teal). In both conformations, the rotation extends from LHCII M2 (state 1) to CP26 (state 10), shown in light grey. **(b)** Differences in the extent of PSII rotation are affected by LHC stromal loops. The stacked $C2S2_{STR}$ (left) state 10 (cyan) is tilted compared to the initial position of state 1 (red), bringing the top dimer closer to the lower dimer, resulting in a shorter range of rotations from CP26 in state 1 to LHCII M2 in state 10.